MiR-204 is responsible for inherited retinal dystrophy associated with ocular coloboma

Conte, Ivan ; Hadfield, Kristen D ; Barbato, Sara ; Carrella, Sabrina ; Pizzo, Mariateresa ; Bhat, Rajeshwari S ; Carissimo, Annamaria ; Karali, Marianthi ; Porter, Louise F ; Urquhart, Jill ; Hateley, Sofie ; O'Sullivan, James ; Manson, Forbes D C ; Neuhauss, Stephan C F ; Banfi, Sandro ; Black, Graeme C M

Abstract: Ocular developmental disorders, including the group classified as microphthalmia, anophthalmia, and coloboma (MAC) and inherited retinal dystrophies, collectively represent leading causes of hereditary blindness. Characterized by extreme genetic and clinical heterogeneity, the separate groups share many common genetic causes, in particular relating to pathways controlling retinal and retinal pigment epithelial maintenance. To understand these shared pathways and delineate the overlap between these groups, we investigated the genetic cause of an autosomal dominantly inherited condition of retinal dystrophy and bilateral coloboma, present in varying degrees in a large, five-generation family. By linkage analysis and exome sequencing, we identified a previously undescribed heterozygous mutation, n.37C > T, in the seed region of microRNA-204 (miR-204), which segregates with the disease in all affected individuals. We demonstrated that this mutation determines significant alterations of miR-204 targeting capabilities via in vitro assays, including transcriptome analysis. In vivo injection, in medaka fish (Oryzias latipes), of the mutated miR-204 caused a phenotype consistent with that observed in the family, including photoreceptor alterations with reduced numbers of both cones and rods as a result of increased apoptosis, thereby confirming the pathogenic effect of the n.37C > T mutation. Finally, knockdown assays in medaka fish demonstrated that miR-204 is necessary for normal photoreceptor function. Overall, these data highlight the importance of miR-204 in the regulation of ocular development and maintenance and provide the first evidence, to our knowledge, of its contribution to eye disease, likely through a gain-of-function mechanism.

DOI: https://doi.org/10.1073/pnas.1401464112

Classification: Biological Sciences: Genetics

MiR-204 is responsible for inherited retinal dystrophy associated with ocular coloboma

Ivan Conte[a,1], Kristen D. Hadfield[b,1], Sara Barbato[a], Sabrina Carrella[a], Mariateresa Pizzo[a], Rajeshwari Bhat[a], Annamaria Carissimo[a], Louise F. Porter [b,c], Jill Urquhart [b,c], Sofie Hateley[b], James O'Sullivan[b], Forbes Manson[b], Stephan C.F. Neuhauss[d], Sandro Banfi[a,e], and Graeme C.M. Black[b,c]

[a]Telethon Institute of Genetics and Medicine, Via Campi Flegrei 34, Pozzuoli (Naples), 80078, Italy;
[b]Manchester Centre for Genomic Medicine, Institute of Human Development, Faculty of Medical and Human Sciences, University of Manchester, Manchester, UK;
[c]Manchester Centre for Genomic Medicine, St Mary's Hospital, Central Manchester University Hospitals NHS Foundation Trust, Manchester Academic Health Sciences Centre, Oxford Road, Manchester, M13 9WL, UK;
[d]Institute of Molecular Life Sciences, University of Zurich, Zurich, Switzerland and
[e]Medical Genetics, Department of Biochemistry, Biophysics and General Pathology, Second University of Naples, Naples, Italy.

[1]These authors contributed equally to this work

Corresponding authors:
Professor Sandro Banfi**,** Telethon Institute of Genetics and Medicine (TIGEM)
Via Campi Flegrei 34, Pozzuoli(Naples), Italy. +39-0816132228, banfi@tigem.it

Professor Graeme Black, Manchester Centre for Genomic Medicine, Institute of Human Development, University of Manchester and Central Manchester University Hospitals NHS Foundation Trust, Manchester Academic Health Sciences Centre (MAHSC), St. Mary's Hospital, Oxford Road Manchester M13 9WL, UK. +44- 161 276 6269, greame.black@manchester.ac.uk.

Keywords: Retinitis pigmentosa, microRNA, retinal degeneration, miR-204, coloboma

Abstract

Ocular developmental disorders, including the group classified as Microphthalmia Anophthalmia and Coloboma (MAC) and inherited retinal dystrophies (IRDs) collectively represent leading causes of hereditary blindness. Characterized by extreme genetic and clinical heterogeneity, the separate groups share many common genetic causes, in particular relating to pathways controlling retinal and retinal pigment epithelial maintenance. In order to understand these shared pathways and delineate the overlap between these groups we investigated the genetic cause of an autosomal dominantly inherited condition of retinal dystrophy and bilateral coloboma, present in varying degrees in a large 5-generation family. By exome sequencing we identified a novel heterozygous mutation, n.37C>T, in the seed region of microRNA-204 (miR-204), which segregates with the disease in all affected individuals. We demonstrated by transcriptome analysis and other *in vitro* assays that this mutation determines significant alterations of miR-204 targeting capabilities. Moreover, we also demonstrated that miR-204 is necessary for proper function of photoreceptor cells as the down-regulation of miR-204 in medaka fish (*Oryzias latipes*) gives rise to an aberrant photoreceptor phenotype with reduced numbers of both cones and rods due to increased apoptosis, which leads to significant alterations of visual function. Finally, we demonstrated *in vivo* the pathogenic effect of the n.37C>T mutation by determining that the injection, in medaka fish, of a mutated miR-204 induced a phenotype consistent with that observed in the family. These data highlight the importance of miR-204 in regulation of ocular development and maintenance and provide the first evidence of its contribution to eye disease.

Significance Statement

MicroRNAs are key players in the regulation of gene expression. An understanding of human conditions caused by microRNA mutations provides insight into mechanisms of gene regulation as well as into the interplay between development and maintenance in tissue homeostasis. The eye represents a preferential target tissue of genetic diseases. Inherited retinal degenerations and developmental eye disorders are two separate groups that represent leading causes of blindness worldwide. Identifying underlying genetic causes of such conditions is important for diagnosis, counselling and potential therapy development. We identified a dominant mutation in microRNA-204 as the genetic cause of a unique phenotype of retinal degeneration and coloboma and thus highlight the importance of miR-204 as a master regulator of ocular development and normal maintenance.

Introduction

The eye represents one of the preferential target tissues of genetic diseases. The main group of genetic disorders affecting the retina is represented by inherited retinal dystrophies (IRD) that include, among others, Retinitis Pigmentosa (RP), one of the leading causes of inherited blindness in the western population with a prevalence of 1:4000 (1). The loss of vision in severe retinal dystrophies is often a result of progressive loss or dysfunction of photoreceptor cells or retinal pigment epithelial (RPE) cells. Besides degenerative disorders, the eye is also the target of a number of developmental genetic disorders, among which the group classified as Microphthalmia Anophthalmia and Coloboma (MAC) feature major structural eye malformations. Both IRDs and MACs are characterized by an extremely high genetic heterogeneity. According to recent estimates, over 150 retinal dystrophy genes (http://www.sph.uth.tmc.edu/Retnet/home.htm) and over 25 MAC genes (http://www.omim.org) have been reported to date, including several that account for conditions in both groups. Many others remain to be identified for both conditions.

MicroRNAs (miRNAs) are emerging as key players in the control of fundamental biological processes in both physiological and pathological conditions. They are single-stranded noncoding, short (20-25 nucleotide) RNAs that regulate gene expression through inhibiting translation of mRNAs or promoting their degradation. Their importance in regulating gene expression in retinal cells is highlighted by the high number of miRNAs that are preferentially expressed in the vertebrate retina (2–5). Evidence indicates that miRNAs are important for development and maintenance of correct function within the eye, and in particular the retina (6–8). Mutations in miRNAs or their target genes may contribute to a range of ocular abnormalities. In this study we investigated the molecular basis for an unusual phenotype observed in a family with a history of varying degrees of retinal degeneration and MAC features (coloboma). We describe the identification of a dominant mutation in miR-204 and demonstrate the functional significance of this mutation to the retinal phenotype observed in this family.

Results

Clinical information

A diagnosis of bilateral coloboma and rod-cone dystrophy with or without cataract was made in 9 individuals of a 5-generation family of Caucasian British descent. Family history suggested an autosomal dominant pattern of inheritance and full clinical examination demonstrated that the phenotype was not associated with extraocular manifestations.

Individual V-1, aged 18 years, was diagnosed with retinal dystrophy and bilateral iris coloboma in early childhood. He had reduced visual acuities (LogMar 0.74 right, 0.84 left) and was registered partially sighted. Mild hypermetropic astigmatism was present (RE +1.75/+o.50 x 100; LE +2.25/+0.50 x 85). Colour vision was seriously compromised bilaterally in City University Colour Vision Test (3rd edition, 1998) and Ishihara colour vision screening test (38 plate edition, 1979). Bilateral iris colobomata with iridolenticular adhesions were present with no evidence of cataract (Fig. 1D). Dilated posterior segment examination revealed scattered retinal pigment epithelium (RPE) mottling with retinal atrophy, attenuation of the retinal vasculature and pale waxy discs bilaterally (Fig. 1E-F). Electroretinography revealed extinguished RE and LE responses to all conditions except a very slight light adapted flicker response (Fig. 1G); 4 years previously this had revealed evidence of a cone response that was now absent. The proband's mother IV-I, aged 42 years, presented with a similar phenotype, having been diagnosed with bilateral iris colobomata and a progressive retinopathy in infancy. She underwent bilateral cataract surgery at the age of 30 years and suffered a retinal detachment in her LE. She was registered blind at age 30 and has hand movement vision in her RE and no perception of light in her LE. Bilateral pseudophakia and posterior capsular opacification gave a limited fundal view (Fig. 1B-C). Individual II-1, III-1, III-2 and III-3 were all registered blind. All had bilateral iris coloboma and a slowly progressive retinal dystrophy leading to marked loss of vision in late childhood or early adult life. Notably, individual III-2 was also found to have congenital cataracts for which underwent right cataract surgery at aged 7 years.

Identification of a miR-204 mutation by linkage analysis and exome sequencing.

To identify possible chromosomal regions associated with the retinal dystrophy and iris coloboma phenotype in this family, parametric linkage analysis was performed for six individuals (Patients II-1, III-1, III-2, V-1, V-2 and V-3), which provided 8 informative meioses. This data achieved a maximal LOD score of 1.81 which falls below the level of 3.0 required to confirm significance of linkage. The data was therefore analysed on the basis of

linkage exclusion for those regions with a LOD score less than -2. There were 4 regions remaining over 5Mb which had a LOD score of between -2 and 1.81 (Fig. S1). Subsequently, exome sequencing was performed on patients II-I and V-I to identify possible causal variants within the potential linked regions. This revealed 39 variant calls common to both patients. To prioritize the likely disease causing mutations we assumed a dominant model of inheritance and excluded homozygous changes. Following further filtering to exclude those variants reported in the Exome Variant Server of the National Heart, Lung, and Blood Institute Exome Sequencing Project (http://evs.gs.washington.edu/EVS/), dbSNP136, 1000 genomes project (www.1000genomes.org), variants which had been previously seen within an in-house database of 244 exomes and those variants confirmed, by sanger sequencing, not to co-segregate with disease in the family resulted in a single novel candidate variant. The n.37C>T mutation identified in the microRNA *MIR204* (reference sequence NR_029621) was an excellent candidate for further study. MiR-204 is preferentially expressed in the eye and several studies have determined its role in eye development (3)(9–11). Evidence of the critical function of miR-204 in eye development strongly suggests a pathogenic role for the mutation identified in this family.

Sanger sequencing confirmed the *MIR204* n.37C>T mutation segregates with the retinal dystrophy and coloboma phenotype in the family members that were tested (II-1, III-1, III-2, III-3, IV-1 and V-1) and absent in the non-affected individuals tested (V-2, V-3) (Fig. 2A). The mutation is positioned at the fourth nucleotide within the highly conserved 7-nucleotide seed region of the 5p arm of the precursor microRNA (annotated according to mirBase,http://mirbase.org (12)) (Fig. 2B). Co-inheritance of retinal dystrophy and MAC is considerably rare. Mutation analysis of an additional 21 cases of known retinal dystrophy with MAC with no family history identified no variants in miR-204. Screening of an additional cohort of 457 patients with isolated MAC and 672 patients with autosomal dominant retinal degeneration phenotypes revealed no novel mutations in miR-204. Moreover, this variant was not present in the control databases of the EVS or 1000 genomes project.

The impact of the n.37C>T mutation on miRNA target recognition

As the *MIR204* mutation identified in our family lies within the seed region of the 5p arm, and therefore in the stem region of pre-miR-204, we used the m-fold algorithm (http://mfold.rit.albany.edu/) (13) to assess how the mutation identified might alter the predicted RNA secondary structure of this microRNA. Although, the n.37C>T mutation introduced a base-pairing mismatch, the decrease in free energy value was small, no bulges were introduced into the RNA structure and the regions critical for Drosha processing of pri-miRNA were not affected (14). Therefore, the n.37C>T mutation was not predicted to destabilise the secondary structure of pre-miR-204 (Fig. 2C). Since mutations in miRNA sequence have been previously reported to alter pre-miRNA processing (15), we examined the impact of the variant on the biogenesis of miR-204. Notably, the expression levels of both the miR-204 and pre-miR-204 species appeared largely unaffected by the n.37C>T mutation (15% increase and 9% decrease, respectively) compared to wild type (Fig. S2). This would suggest an alternative mechanism for the pathogenesis of this dominantly inherited mutation.

Since the mutation lies within the seed region of the mature miRNA, it was more likely that this change would affect recognition of target genes. This could occur through two different modalities, i.e., either impaired recognition of *bona fide* miR-204 targets (loss-of-function mechanism) or creation of novel aberrant target sites (gain-of-function mechanism). To evaluate the relative contribution of either of the above mechanisms, we carried out a microRNA target prediction with the TargetScan (www.targetscan.org) and Diana-*microT (*diana.cslab.ece.ntua.gr/microT/*)* tools using as query the miR-204 sequence containing the n.37C>T variant. Intriguingly, we found that the mutated miR-204 sequence was predicted to target a much higher number of mRNAs (n=1132) vs. the wild-type sequence (n=557) (Table S1). Only 135 mRNA were predicted to be targeted by both the wild-type (wt) and the mutated (mut) miR-204 sequence suggesting that the n.37C>T sequence variant could indeed cause a notable alteration of miR-204 targeting properties. Luciferase assays or real-time RT-PCR assays on a subset of targets validated some of the above predictions in all examples tested (Fig. S2).

Therefore, in order to obtain a more global assessment of the effect of the n.37C>T sequence variant in the miR-204 sequence, we carried out transcriptome analysis by RNAseq analysis in a human RPE cell line (ARPE-19) (16). In particular, we transfected the cells with miR-204 mimics corresponding to either the wild-type (wt) or to the mutated (mut) sequence and compared the results obtained from their RNAseq transcriptome profiles. We found that the

number of significantly down-regulated genes vs. a negative mimic control (false discovery rate<0.05) was higher in mut-miR-204-transfected (n=2129) than in wt-miR-204-transfected (n=1487) ARPE-19 cells. More importantly, we observed that genes down-regulated in cells transfected with wt-mimics were significantly and specifically enriched for wt-miR-204 targets (n=154; hypergeometric p-value=2.90E-60) and that, conversely, genes downregulated in cells transfected with mut-mimics were significantly and specifically enriched for mut-miR-204 targets (n=249; hypergeometric p-value=3.31E-47) (Fig. 3). We found that out of the 154 wt-miR-204 predicted targets displaying a statistically significant decrease of their expression levels vs. controls in wt-miR-204-transfected cells, only 48 behaved similarly in mut-miR-204-transfected cells. On the other hand, out of the 249 mut-miR-204 predicted targets displaying a statistically significant decrease of their expression levels vs. controls in mut-miR-204-transfected cells, only 72 displayed a similar trend in wt-miR-204 transfected cells. Overall, these data confirmed that the n.37C>T mutation determines a significant alteration of miR-204 function by both generating a large number of novel and aberrant direct targets (gain-of-function mechanism) and by impairing the recognition of wild-type targets (loss-of-function mechanism).

MiR-204 knockdown induces an aberrant photoreceptor phenotype in vivo

MiR-204 has been described to have a significant role in eye development. We previously reported that knockdown of this microRNA in medaka fish was linked to microphthalmia, abnormal lens development and eye coloboma (9, 17). However, an involvement of miR-204 in photoreceptor function was never described. To further support the pathogenic role of this miRNA in the phenotype observed in our family, we performed miR-204 inactivation in medaka fish using morpholino (Mo) oligonucleotides, as previously described (9, 17), and assessed the consequences in the differentiated retina.

Comparison of the morphology of the differentiated retina of control and Mo-miR-204-injected embryos revealed that morphant retinas displayed significant alteration in photoreceptor marker staining, which was more evident in ventral regions (Fig. 4A-D'). In particular, we observed by immunofluorescence a significant reduction of rhodopsin-positive mature rod photoreceptors and of Zpr-1-positive mature cone photoreceptors (Fig. 4A-D'). The significant down-regulation of photoreceptor markers was also confirmed at the transcript level for both the *Oryzias latipes* (*ol) olRho* and *olCrx* genes (Fig. S3). The above defects were more evident in morphant embryos that also displayed coloboma, in which

photoreceptor cells were completely absent in the ventral retina. On the other hand, we did not observe in morphant fish any apparent alterations in the number of other retinal neuronal cells, as determined by expression analysis of *olOtx2*, *olPax6* and *olProx1* (Fig. S3).

The above data indicate that miR-204 knockdown causes a significant reduction of photoreceptor cells in medaka fish. We considered whether this reduction could be due to either alteration of cell proliferation or to apoptosis. At the optic cup stage and during retinal differentiation, immunostaining for phosphorylated histone H3 (PH-3), a specific marker for cells in the M-phase of cell cycle, revealed no difference in the number of proliferating retinal cells in miR-204 morphants when compared to control embryos (Fig. 4F-H). In contrast, at the onset of photoreceptor cell differentiation (St30-33), a significant increase in the number of TUNEL-positive apoptotic cells was detected in the retinas of miR-204 morphants when compared to controls (Fig. 4I-K) thus suggesting that the reduction of photoreceptor cells in miR-204 morphant fish is mostly due to increased apoptosis.

Finally, we performed a detailed analysis of photoreceptor function in miR-204 morphant larvae. We recorded flash electroretinogram (ERG) under scotopic conditions from both control and miR-204 morphant larvae. Notably, we observed a significant reduction of the amplitude of the b-wave in miR-204 morphant compared to control medaka larvae (n=30) (Fig. 4E). The amplitude reduction was consistently observed at all luminance values analyzed. These data indicate that the loss of photoreceptors caused by miR-204 knockdown determines a significant alteration of visual function.

Injection of the n.37C>T mutated miR-204 causes severe ocular malformations associated with retinal dystrophy in vivo.

To test *in vivo* the putative pathogenic effect of the miR-204 n.37C>T variation, we overexpressed a miR-204 mimic carrying the mutation (mut-miR-204) in medaka fish. Embryos injected with mut-miR-204 at the one-cell stage showed an aberrant eye phenotype (90 ± 5% of 1,500 injected embryos) from St19, corresponding to optic vesicle formation, onward. In particular, growth of the eye cup was significantly impaired and culminated at St38 in evident microphthalmia and optic coloboma (Fig. 5B). These phenotypic alterations were very different and much more severe with respect to those observed after overexpression in medaka of a wild-type miR-204 mimic only characterized by a modest microphthalmia (Fig. 5C). Moreover, to assess whether the n.37C>T variation also had an

effect on photoreceptor development, we analyzed the retinas of mut-miR-204 injected embryos at St.38 (n = 20 eyes). We observed a notable reduction of both rod and cone photoreceptor cells in mut-miR-204 overexpression in comparison to both wt-miR-204 and control injected embryos, as assessed by immunofluorescence analysis with an anti-Rhodopsin and anti-Zpr-1 antibodies (Fig. 5D-I), respectively. Overall, the above data further confirm also *in vivo* that the n.37C>T variation significantly alters miR-204 function and then strengthen its pathogenic role in the complex phenotype observed in our family. Finally, these *in vivo* studies uncover, for the first time, the essential role of miR-204 in photoreceptor cell differentiation and function (Fig. 4 and 5).

Discussion

In this study we describe a five-generation family with an overlapping phenotype of inherited retinal dystrophy and optic fissure closure defect, iris coloboma. To elucidate the underlying molecular basis of this phenotype we undertook a combined linkage and exome sequencing approach identifying 4 potentially linked regions one of which, on chromosome 9q21, contained a novel heterozygous mutation in *MIR204* (n.37C>T) that segregated with the phenotype observed in this family. Given the well-documented role of miR-204 in eye development, this mutation was a strong candidate for further investigation.

MiR-204 has discrete and dynamic expression domains in the eye throughout development, being expressed in the RPE, neural retina, lens and ciliary body in fish, mouse and human (3, 4, 10, 11, 18–20). A large body of evidence indicates that miR-204 plays a crucial role in the differentiation and function of all the ocular structures in which it is expressed. *In vitro* assays have shown that miR-204 may be involved in the correct differentiation and function of RPE cells (19, 21, 22). MiR-204 is also required for proper lens development (9, 10). We previously reported that this action is exerted through a complex cross-talk with the transcription factor Pax6, a 'master regulator' of eye development. We found that while Pax6 controls the expression of miR-204 (11), miR-204 can itself repress Pax6 through the targeting of the transcription factor *Meis2* (10). Additional target genes that play a role in miR-204 action in lens differentiation are *Ankrd13a* (9), *Sox11* (11) and *Hmx1* (23). Finally, miR-204 controls the establishment of the proper dorsal-ventral axis and its inactivation was linked to coloboma in medaka fish (10).

In spite of its pervasive role in many aspects of ocular differentiation, miR-204 has not previously been reported to have an impact on photoreceptor function. Here, we demonstrate that knockdown of miR-204 function in medaka fish leads to progressive alteration and death of photoreceptor cells (Fig. 4). These alterations translate into profound abnormalities of photoreceptor and visual function as determined by ERG analysis (Fig. 4E). These data strongly indicate that miR-204 is also required for photoreceptor development and function. It is important to point out that miR-204 has not been previously reported to be significantly expressed in photoreceptor cells by RNA *in situ* hybridization assays (3, 11, 17, 18, 20). Therefore, it is possible to hypothesize either a cell autonomous action of this miRNA in photoreceptors, i.e., by being expressed at low levels at crucial developmental stages or a non-cell autonomous action. The latter may be mediated by the remarkable expression of miR-204 in the RPE (3, 11, 20). There are many examples of RPE-specific genes that play essential roles in photoreceptor function and whose mutations have pathogenic role in inherited retinal dystrophies (24, 25). In any case, the dissection of the molecular mechanisms through which miR-204 regulates photoreceptor function requires further studies.

This is the first report of a pathogenic mutation within miR-204 identified as the cause of an ocular disease. It is supported by two main considerations. First, the n.37C>T mutation falls within the mature miR-204 seed region, which is considered to be the most essential sequence domain for target recognition and down-regulation (26). We demonstrate *in vitro* that this variation has an impact on target mRNA recognition (Fig. 3 and Fig. S2), which would be anticipated to lead to significant dysregulation of gene expression in eye tissues involving both natural or aberrantly generated miR-204 targets. Second, we demonstrated that the n.37C>T variation has a deleterious effect *in vivo*. In particular, we found that the overexpression of a miR-204 mimic carrying the n.37C>T mutation in medaka fish generates a dramatic eye phenotype characterized by gross malformations (including microphthalmia and coloboma) and photoreceptor abnormalities (Fig. 5). These results not only clearly support the deleterious role played by the n.37C>T mutation but also support its pathogenic role in the complex form of retinal dystrophy observed in the family we report in this study.

We have identified a miR-204 mutation in a single large, family. We did not identify this mutation, or additional miR-204 mutations, in patients with either isolated IRD or MAC – that is phenotypes partly overlapping that observed in our family. However, the combination of retinal dystrophy and ocular coloboma is very rarely observed in clinical practice, in

particular when inherited as an autosomal dominant trait. It is therefore conceivable that this particular miR-204 mutation underlies the pathogenesis of an extremely rare ocular condition. This is in line with the limited number of reports of mutations within microRNAs associated with Mendelian disorders to date. The first report of mutations within a miRNA contributing to a disease phenotype was by Mencía *et al*., who identified two point mutations within the seed region of miR-96, which segregated with the affected patients from two separate Spanish families with autosomal dominant progressive hearing loss (27). The resulting mutations directly affected the miR-96 biogenesis and resulted in a significant reduction in the silencing of target genes. Soldà *et al*. reported a mutation in the 3p arm of *MIR96* in a family with non-syndromic inherited hearing loss (15). This mutation was found to impair correct maturation of miR-96 leading to a significant decrease in the expression level of the mature 3p and 5p microRNA arms. The only other example of a microRNA with point mutations being associated with a Mendelian disorder is represented by *MIR184*. Hughes *et al*. identified a mutation in the central nucleotide of the seed region of *MIR184* as the cause of keratoconus and early-onset anterior polar cataracts in a large Irish family (28). Iliff *et al*. reported the same mutation as the cause of EDICT syndrome, an autosomal dominant anterior segment dysgenesis syndrome characterized by endothelial dystrophy, iris hypoplasia, congenital cataract and stromal thinning (29). A further two novel heterozygous substitution variants, neither of which were located within the seed region, were later identified in *MIR184* in two patients with isolated keratoconus (30). This is also the first report of a microRNA mutation with a causative role in inherited retinal dystrophies in patients as, to date, microRNAs have been linked to such diseases only in mouse (31).

There are several reasons to explain the paucity of genetic diseases caused by miRNA mutations. First, given their shortness it is expected that the number of potential mutations affecting miRNA mature sequences will be significantly lower when compared to that of mutations falling within functional sequence elements of protein coding genes. Second, given the fact that each miRNA can target hundreds of different genes, mutations affecting critical nucleotides of mature sequences may give rise to phenotypes that depend on the target specificity affected by each mutation. Mutations altering miRNA function may not only be localized within their mature sequences but also in their binding sites within the 3'-UTR of target genes, as described in the cases of spastic paraplegia (32) and X-linked chondrodysplasia (33). Such mutations in the 3' UTR would be expected to selectively affect specific aspects of miRNA actions and consequently to give rise to disease phenotypes that

will differ from those observed when mutations lie in the miRNA sequence itself. The assessment of the true impact of 3'-UTR mutations on genetic disorders will require analysis of gene regions thus far neglected in mutation screens.

The n.37C>T mutation results in an autosomal dominantly inherited phenotype and thus could act either through loss-of-function (i.e. by impairing recognition of wild-type miR-204 targets) or gain-of-function (by creating novel aberrant recognition sites in genes that should not normally be targeted by miR-204) mechanisms. We hypothesize that the gain-of-function mechanism exerts a predominant role for the following three reasons. First, both bioinformatic predictions and transcriptome studies indicate that the n.37C>T mutation is able to generate a much larger dataset of predicted targets as compared with the wild-type miR-204 mature sequence. Second, the injection in medaka fish of the mutated miR-204 leads to a striking eye phenotype, much more severe than that obtained with injection of the wild-type miR-204. Finally, there are previous clinical data that seem to further exclude haploinsufficiency. MiR-204 is located within intron 8 of the transient receptor potential (TRP) channel gene, *TRPM3* on chromosome 9q21.12. Deletions within 9q21 and those specifically encompassing the *TRPM3* gene have not been reported to cause ocular phenotypes, instead features of mental retardation, epilepsy, speech delay, autistic behaviour and moderate facial dysmorphology (34–37). Deletion of this region has been described in association with an autism phenotype in a family in which a paternal deletion of exons 1–9 of TRMP3, that included *MIR204*, was shared by two affected sons and an unaffected daughter who were not described to have an ocular phenotype or visual symptoms. Furthermore, at least 30 patients with deletions in this region are listed on the Decipher database, a web-based resource and database of genomic copy number variation data from analysis of patient DNA; none is described with coloboma or retinal disease although one had optic nerve hypoplasia. Altogether, the above data indicate that the n.37C>T mutation mostly acts with a gain-of-function mechanism although we cannot exclude that the loss of some miR-204 wild-type targets may still contribute to the phenotype observed in our family.

Based on the above observations, we hypothesize that miR-204 is likely to play a key role in the pathogenesis of human eye diseases not only by means of different mutations in its mature sequence but also potentially through variation in recognition sites in some of its most relevant targets.

In summary, we have identified a new genetic cause for the pathogenesis of complex forms of eye diseases, particularly characterized by the combination of retinal dystrophy and developmental abnormalities. Our findings contribute to highlight miR-204 as a new putative "master regulator" of eye development, and in particular have been instrumental in uncovering its newly identified role in photoreceptor survival and function. Finally, our results shed further light on the recognition of the role of miRNAs as primary pathogenic agents in human genetic diseases.

Materials and Methods

Subjects

A single 5-generation family with a highly unusual and visually disabling phenotype consisting of retinal dystrophy, and bilateral iris coloboma presented at the retinal and genetic clinic of the Manchester Royal Eye Hospital (Manchester, UK). A total of 9 family members exhibited a similar phenotype (6 female and 3 male) (Fig. 1A). To elucidate the molecular basis of this phenotype we enrolled 8 family members for clinical and molecular genetic analysis, including 6 affected individuals. Ethical approval and informed consent was obtained from all study participants. The research adhered to the tenets of the Declaration of Helsinki.

Disease status was determined by a full medical, ophthalmic and family history combined with clinical examination and electrophysiological evidence in proband V-1, and his mother, patient IV-1. Medical records for other family members were reviewed with the patients' written consent. Ophthalmic examination included anterior segment examination by slit lamp biomicroscopy with evaluation of anterior chamber depth using the Von Herrick method, intra-ocular pressure measurements, and dilated fundus examination and photography. Optical coherence tomography (OCT) for retinal thickness assessment using the Heidelberg spectral-domain OCT (Heidelberg engineering) was performed with autofluorescence and colour imaging. Full-field flash electroretinograms (ERG) were also carried out in individual V-1. Individual IV-1 underwent ERG testing in the 1980s. ERGs were recorded following the standards of the International Society for Clinical Electrophysiology of Vision (ISCEV) (38). Both scotopic rod-driven responses and cone-driven photopic single flash and 30-Hz flicker stimuli were recorded sequentially.

Linkage analysis

Genome-Wide SNP analysis was carried out using the Affymetrix Genome-Wide SNP6.0 microarray. Genotypes were generated using the genotyping console software provided by Affymetrix using the Birdseed V2 algorithm and a confidence threshold of 0.005. A subset of SNPs were selected for linkage analysis based on having a MAF of 0.2 in order to reduce the problems associated with linkage disequilibrium when using dense marker sets. Parametric multipoint linkage analysis was performed using Merlin (http://www.sph.umich.edu/csg/abecasis/merlin/index.html) using a dominant model with full penetrance.

Exome sequencing and variant prioritization

Whole-exome target enrichment and sequencing were performed on 3 ug of DNA extracted from peripheral blood of two affected family members, proband V-I and patient II-I (Fig. 1A). For patient V-I enrichment was performed using the SureSelect Human All Exon v.1 Enrichment kit (Agilent Technologies, Santa Clara, CA, USA) for the Illumina HiSeq system, according to the manufacturer's protocol. Sequencing was carried out on a HiSeq 2000 sequencer (Illumina Inc, San Diego, CA, USA), following the manufacturer's protocols by Hong Kong Co. Hong Kong. Sequence data were mapped to the hg19 reference human genome using BWA software. Variants were called using GATK v2.4.7 software then filtered for those SNPs with ≤ 5X coverage. Approximately 4 GB of sequence mapped uniquely to the genome reference hg19, with 69.4% of the exome covered at 20-fold or higher. SNPs and insertions/deletions were initially annotated to genes using Ensembl v68 and the functional consequences were then defined against an in-house list of Refseq transcripts (www.ncbi.nlm.nih.gov/refseq). Using Ensembl's defined consequence hierarchically system, the highest impacting consequence for a variant in a gene was retained. To find likely pathogenic changes an in-house hierarchy system of functional consequence was used to prioritize variants, as detailed in (39). Briefly, variants were filtered out if they were present in dbSNP136 (unless seen in the Human Gene Mutation Database (HGMD), http://www.hgmd.org), if seen more than once in our in-house variant database, present in the 1000 genomes project or the exome variant server (EVS). Novel changes were analysed further using the in-silico tools SIFT (Sorting Intolerant from Tolerant) (40), PolyPhen-2 (41), and splicing prediction tools via the software Alamut (Interactive Biosoftware, LLC) to assess their pathogenicity.

For patient II-1, enrichment was performed using TargetSeq exome enrichment (Life Technologies, Carlsbad, CA, USA) following the manufacturer's protocols. Emulsion PCR was conducted on the resultant enriched sample library and the sample was run indexed with unrelated samples on a SOLiD 5500xl sequencer following the manufacturer's protocols. Sequence data were mapped to the hg19 reference human genome using Lifescope software. Approximately 4.5 GB of sequence mapped uniquely to the genome reference hg19, with 68.2% of the exome covered at 20-fold or higher. Variants were called using a combination of the Lifescope software suite and SAMtools (freeware)(42) and then filtered for those SNPs with ≤ 5X coverage. SNPs were annotated and filtered as for patient V-I.

*PCR and Sanger sequencing to confirm novel variant*s

Mutations identified in candidate genes by exome sequencing were confirmed by direct Sanger sequencing. PCR amplification of *MIR204* was performed using the oligonucleotide primers listed in Table S2. Amplicons were sequenced using the BigDye Terminator v3.1 system (Life Technologies) and analysed on an ABI 3730 DNA Analyser (Life Technologies).

Cell transfections, RNA extraction and analysis

ARPE-19 cells (16) were cultured at 37ºC in a humidified chamber supplemented with 5% CO_2. Cells were seeded at 135000 cell/mL in 24-multi well plates and transfected with DNA constructs using the PolyFect transfection reagent (Qiagen) according to the manufacturer's instructions. Total RNA was extracted using TRIZOL (Invitrogen) according to the manufacturer's instructions and used for subsequent RNA-Seq-based profiling as previously described (43). RNA-Seq libraries were generated following the standard Illumina RNASeq protocol and sequenced using an Illumina HiSeq 1000 at the Next Generation Sequencing Facility of the Telethon Institute of Genetics and Medicine. Differential expression analysis of read counts was performed using the Generalized Linear Model approach for multiple groups implemented in the Bioconductor package "edgeR" (44, 45). The expression cutoff used was 1 CPM (Count Per Million) in at least three samples.

HeLa cell and H36CE human lens epithelial (46) cell lines were cultured at 37ºC in a humidified chamber supplemented with 5% CO_2 as previously described (9). Cells were seeded at 135000 cell/mL in 24-multi well plates and transfected with DNA constructs using the PolyFect transfection reagent (Qiagen) according to the manufacturer's instructions.

pGL3-TK plasmids containing the 3' UTR of the human *MEIS2* and *ANKRD13A* mRNAs and psiUx plasmid constructs containing the wild-type or the mutated form of precursor sequences of hsa-miR-204 were generated and used in luciferase assays as previously described (9, 10). For quantitative RT-PCR experiments, H36CE cells were transfected with psiUx plasmid constructs containing the wild-type or the mutated form of precursor sequences of hsa-miR-204 and qRT-PCR were performed as described (9). Each assay was performed in duplicate and results are presented as mean ± SD for at least three independent assays. The primers used for the qRT-PCR are listed in Table S3.

Quantitative RT-PCR to assess biogenesis of miR-204

psiUx plasmid constructs containing the wild-type or the mutated form of precursor sequences of hsa-miR-204, generated as previously described (9, 10), were transfected into ME-180 (47) cells using Lipofectamine 2000 (Life Technologies) according to the manufacturer's instructions. RNA was extracted after 24 h, using the miRNeasy isolation kit (Qiagen). Reverse transcription was performed using the Taqman® MicroRNA reverse transcription kit (Life Technologies) with specific custom designed stem loop RT primers for the mature mir-204 and precursor mir-204 products (Table S4). Real-Time PCR was performed using FastStart Universal SYBR Green Master mix (Roche Applied Sciences) and miRNA specific forward and reverse primers listed in Table S4. Expression of U6 snRNA, used to normalise RNA input, was assessed using a TaqMan® Small RNA assay (Life Technologies), according to the manufacturer's instructions. Expression values were generated using a standard curve method. In all experiments miR-98 was used as an internal control to normalise for transfection efficiency. Each assay was performed in triplicate and data is presented as the mean ±SD of three individual experiments.

Medaka stocks and miR-204 mimic morpholino injections.

The Cab-strain of wild-type medaka fish (*Oryzias latipes*) were maintained as previously described (9). Embryos were staged according to Iwamatsu *et al*. (48). Morpholinos (Gene Tools, LLC, OR) and both wild-type and mutated miRIDIAN Dharmacon miR-204 mimics were designed and injected into one-cell fertilized embryos as previously described (10). All fish studies were conducted in strict accordance with the institutional guidelines for animal research and approved by the Italian Ministry of Health.

RNA in situ hybridization and immunofluorescence.

Whole-mount RNA *in situ* hybridizations were performed, photographed and sectioned (25-µm vibratome sections) as described by Conte *et al*. (17). Digoxigenin-labeled anti-sense and sense riboprobes for *olCrx, olPax6, olOtx2* and *olRhodopsin* were used (17). Medaka embryos were cryostat-sectioned (12-µm) and immuno-labeling was performed as previously described (17) using mouse monoclonal antibodies to Rhodopsin (Rho) (1:2000, Sigma) and Zpr-1 (1:2000, ZIRC) and the rabbit polyclonal antibody to Prox1 (1:200, Chemicon). Alexa-488-conjugated goat α-mouse and goat α-rabbit (1:1000, Invitrogen) secondary antibodies were used. For the cell proliferation analysis, rabbit α-phospho-histone H3 (1:100, Cell signaling Technology) and peroxidase-conjugated anti-rabbit antibody (1:200, vector laboratories) were used followed by DAB staining as previously described (49). Confocal images were acquired using the Zeiss microscope, LSM 710.

Detection of apoptotic cell death

The extent and distribution of apoptotic cell death was determined by TdT-mediated dUTP nick end labeling (TUNEL), using the In Situ Cell Death Detection Kit, POD (Roche) following the manufacturer's protocol.

Fish Electroretinogram.

Electroretinograms (ERGs) were recorded as described previously (50). Briefly, medaka larvae were dark adapted for 30 min. For recording, a reference electrode was placed in a 1% agarose in ddH_2O. The larva was placed dorsal-up on a moist paper covering the reference electrode. The recording electrode with a tip diameter of approximately 20 µm was filled with buffer E3 (5 mM NaCl, 0.17 mM KCl, 0.33 mM CaCl2, and 0.33 mM MgSO4) and placed on the cornea of the larva. Light stimuli of 100 ms with interstimulus intervals of 7 s were applied. The light stimulus intensity was 665 lux.

Acknowledgements

We thank Francesco Salierno and Jinjing Zang for technical assistance. Members of the European retinal dystrophy consortium (ERDC) who contributed to this work are Frans Cremers, Carmen Ayuso, Susanne Kohl, Bernd Wissinger, Carlo Rivolta, Chris Inglehearn, Carmel Toomes, Dror Sharon and Robert K. Koenekoop. We are grateful to David Fitzpatrick and Daniel Schorderet for study of ocular developmental disorders. We thank Dr

Neil Parry who performed and interpreted the patient ERGs, the TIGEM Bioinformatics and the TIGEM Next Generation Sequencing cores for technical assistance in the generation and analysis of the transcriptome data. This work was supported by funding from the National Institute for Health Research's Manchester Biomedical Research Centre a programme grant from Fight for Sight (grant number 1801), funding support from RP Fighting Blindness, funding from the Italian Telethon Foundation (grant TGM11SB2). Sara Barbato was the recipient of an EMBO short-term fellowship and of a fellowship from the Company of Biologists Ltd. The authors have no conflicts of interest to declare.

References

1. Wright AF, Chakarova CF, Abd El-Aziz MM, Bhattacharya SS (2010) Photoreceptor degeneration: genetic and mechanistic dissection of a complex trait. *Nat Rev Genet* 11(4):273–284.

2. Arora A, et al. (2010) Prediction of microRNAs affecting mRNA expression during retinal development. *BMC Dev Biol* 10:1.

3. Karali M, Peluso I, Marigo V, Banfi S (2007) Identification and characterization of microRNAs expressed in the mouse eye. *Invest Ophthalmol Vis Sci* 48(2):509–515.

4. Karali M, et al. (2010) miRNeye: a microRNA expression atlas of the mouse eye. *BMC Genomics* 11:715.

5. Ryan DG, Oliveira-Fernandes M, Lavker RM (2006) MicroRNAs of the mammalian eye display distinct and overlapping tissue specificity. *Mol Vis* 12:1175–1184.

6. Damiani D, et al. (2008) Dicer inactivation leads to progressive functional and structural degeneration of the mouse retina. *J Neurosci Off J Soc Neurosci* 28(19):4878–4887.

7. La Torre A, Georgi S, Reh TA (2013) Conserved microRNA pathway regulates developmental timing of retinal neurogenesis. *Proc Natl Acad Sci U S A* 110(26):E2362–2370.

8. Conte I, Banfi S, Bovolenta P (2013) Non-coding RNAs in the development of sensory organs and related diseases. *Cell Mol Life Sci CMLS* 70(21):4141–4155.

9. Avellino R, et al. (2013) miR-204 targeting of Ankrd13A controls both mesenchymal neural crest and lens cell migration. *PloS One* 8(4):e61099.

10. Conte I, et al. (2010) miR-204 is required for lens and retinal development via Meis2 targeting. *Proc Natl Acad Sci U S A* 107(35):15491–15496.

11. Shaham O, et al. (2013) Pax6 regulates gene expression in the vertebrate lens through miR-204. *PLoS Genet* 9(3):e1003357.

12. Griffiths-Jones S, Saini HK, van Dongen S, Enright AJ (2008) miRBase: tools for microRNA genomics. *Nucleic Acids Res* 36(Database issue):D154–158.

13. Zuker M (2003) Mfold web server for nucleic acid folding and hybridization prediction. *Nucleic Acids Res* 31(13):3406–3415.

14. Han J, et al. (2006) Molecular basis for the recognition of primary microRNAs by the Drosha-DGCR8 complex. *Cell* 125(5):887–901.

15. Soldà G, et al. (2012) A novel mutation within the MIR96 gene causes non-syndromic inherited hearing loss in an Italian family by altering pre-miRNA processing. *Hum Mol Genet* 21(3):577–585.

16. Dunn KC, Aotaki-Keen AE, Putkey FR, Hjelmeland LM (1996) ARPE-19, a human retinal pigment epithelial cell line with differentiated properties. *Exp Eye Res* 62(2):155–169.

17. Conte I, et al. (2010) Proper differentiation of photoreceptors and amacrine cells depends on a regulatory loop between NeuroD and Six6. *Dev Camb Engl* 137(14):2307–2317.

18. Xu S, Witmer PD, Lumayag S, Kovacs B, Valle D (2007) MicroRNA (miRNA) transcriptome of mouse retina and identification of a sensory organ-specific miRNA cluster. *J Biol Chem* 282(34):25053–25066.

19. Wang FE, et al. (2010) MicroRNA-204/211 alters epithelial physiology. *FASEB J Off Publ Fed Am Soc Exp Biol* 24(5):1552–1571.

20. Deo M, Yu J-Y, Chung K-H, Tippens M, Turner DL (2006) Detection of mammalian microRNA expression by in situ hybridization with RNA oligonucleotides. *Dev Dyn Off Publ Am Assoc Anat* 235(9):2538–2548.

21. Li W-B, et al. (2012) Development of retinal pigment epithelium from human parthenogenetic embryonic stem cells and microRNA signature. *Invest Ophthalmol Vis Sci* 53(9):5334–5343.

22. Adijanto J, et al. (2012) Microphthalmia-associated transcription factor (MITF) promotes differentiation of human retinal pigment epithelium (RPE) by regulating microRNAs-204/211 expression. *J Biol Chem* 287(24):20491–20503.

23. Li X-Y, Zhang K, Jiang Z-Y, Cai L-H (2014) MiR-204/miR-211 downregulation contributes to candidemia-induced kidney injuries via derepression of Hmx1 expression. *Life Sci* 102(2):139–144.

24. Davidson AE, et al. (2009) Missense mutations in a retinal pigment epithelium protein, bestrophin-1, cause retinitis pigmentosa. *Am J Hum Genet* 85(5):581–592.

25. Thompson DA, et al. (2001) Mutations in the gene encoding lecithin retinol acyltransferase are associated with early-onset severe retinal dystrophy. *Nat Genet* 28(2):123–124.

26. Lewis BP, Burge CB, Bartel DP (2005) Conserved seed pairing, often flanked by adenosines, indicates that thousands of human genes are microRNA targets. *Cell* 120(1):15–20.

27. Mencía A, et al. (2009) Mutations in the seed region of human miR-96 are responsible for nonsyndromic progressive hearing loss. *Nat Genet* 41(5):609–613.

28. Hughes AE, et al. (2011) Mutation altering the miR-184 seed region causes familial keratoconus with cataract. *Am J Hum Genet* 89(5):628–633.

29. Iliff BW, Riazuddin SA, Gottsch JD (2012) A single-base substitution in the seed region of miR-184 causes EDICT syndrome. *Invest Ophthalmol Vis Sci* 53(1):348–353.

30. Lechner J, et al. (2013) Mutational analysis of MIR184 in sporadic keratoconus and myopia. *Invest Ophthalmol Vis Sci* 54(8):5266–5272.

31. Lumayag S, et al. (2013) Inactivation of the microRNA-183/96/182 cluster results in syndromic retinal degeneration. *Proc Natl Acad Sci U S A* 110(6):E507–516.

32. Züchner S, et al. (2006) Mutations in the novel mitochondrial protein REEP1 cause hereditary spastic paraplegia type 31. *Am J Hum Genet* 79(2):365–369.

33. Simon D, et al. (2010) A mutation in the 3'-UTR of the HDAC6 gene abolishing the post-transcriptional regulation mediated by hsa-miR-433 is linked to a new form of dominant X-linked chondrodysplasia. *Hum Mol Genet* 19(10):2015–2027.

34. Boudry-Labis E, et al. (2013) A novel microdeletion syndrome at 9q21.13 characterised by mental retardation, speech delay, epilepsy and characteristic facial features. *Eur J Med Genet* 56(3):163–170.

35. Bartnik M, et al. (2012) Application of array comparative genomic hybridization in 102 patients with epilepsy and additional neurodevelopmental disorders. *Am J Med Genet Part B Neuropsychiatr Genet Off Publ Int Soc Psychiatr Genet* 159B(7):760–771.

36. Pua HH, et al. (2014) Novel interstitial 2.6 Mb deletion on 9q21 associated with multiple congenital anomalies. *Am J Med Genet A* 164A(1):237–242.

37. Baglietto MG, et al. (2014) RORB gene and 9q21.13 microdeletion: report on a patient with epilepsy and mild intellectual disability. *Eur J Med Genet* 57(1):44–46.

38. Marmor MF, et al. (2009) ISCEV Standard for full-field clinical electroretinography (2008 update). *Doc Ophthalmol Adv Ophthalmol* 118(1):69–77.

39. Gillespie RL, et al. (2014) Personalized Diagnosis and Management of Congenital Cataract by Next-Generation Sequencing. *Ophthalmology*.

40. Kumar P, Henikoff S, Ng PC (2009) Predicting the effects of coding non-synonymous variants on protein function using the SIFT algorithm. *Nat Protoc* 4(7):1073–1081.

41. Adzhubei IA, et al. (2010) A method and server for predicting damaging missense mutations. *Nat Methods* 7(4):248–249.

42. Li H, et al. (2009) The Sequence Alignment/Map format and SAMtools. *Bioinforma Oxf Engl* 25(16):2078–2079.

43. Conte I, et al. (2014) The combination of transcriptomics and informatics identifies pathways targeted by miR-204 during neurogenesis and axon guidance. *Nucleic Acids Res* 42(12):7793–7806.

44. Gentleman RC, et al. (2004) Bioconductor: open software development for computational biology and bioinformatics. *Genome Biol* 5(10):R80.

45. Robinson MD, McCarthy DJ, Smyth GK (2010) edgeR: a Bioconductor package for differential expression analysis of digital gene expression data. *Bioinforma Oxf Engl* 26(1):139–140.

46. Porter RM, Hutcheson AM, Rugg EL, Quinlan RA, Lane EB (1998) cDNA cloning, expression, and assembly characteristics of mouse keratin 16. *J Biol Chem* 273(48):32265–32272.

47. Sykes JA, Whitescarver J, Jernstrom P, Nolan JF, Byatt P (1970) Some properties of a new epithelial cell line of human origin. *J Natl Cancer Inst* 45(1):107–122.

48. Iwamatsu T (2004) Stages of normal development in the medaka Oryzias latipes. *Mech Dev* 121(7-8):605–618.

49. Beccari L, Conte I, Cisneros E, Bovolenta P (2012) Sox2-mediated differential activation of Six3.2 contributes to forebrain patterning. *Dev Camb Engl* 139(1):151–164.

50. Makhankov YV, Rinner O, Neuhauss SCF (2004) An inexpensive device for non-invasive electroretinography in small aquatic vertebrates. *J Neurosci Methods* 135(1-2):205–210.

Figure legends

Fig. 1. Ocular phenotype of family with inherited retinal dystrophy and iris coloboma. A) Pedigree of family. The proband is denoted by an arrow. * denotes patients affected with retinal dystrophy and coloboma who underwent exome sequencing. • denotes all patients where DNA was available for testing. B-D) Slit lamp biomicroscopy photographs of affected family members. Right (B) and left eye (C) of patient IV-I demonstrating inferior iris coloboma and iridolenticular adhesions. Left eye of patient V-I (D) shows inferior iris coloboma and evidence of iridolenticular adhesions but no evidence of significant cataract. E) Fundus photograph of the retina of patient V-1, showing extensive chorioretinal atrophy and retinal pigment epithelium mottling. F) Cross-sectional OCT image taken with the Heidelberg Spectralis scanning laser ophthalmoscope with enhanced depth imaging features. Retinal thinning as a result of loss of inner and outer photoreceptor segments is evident. There is focal disturbance of the retinal pigment epithelium layer. G) Electroretinogram of left and right eye of patient V-1 demonstrating extinguished responses to all conditions except a very slight light adapted flicker response (upper part of diagram). Shaded areas represent 95% confidence intervals

Fig. 2. The novel miR-204 mutation (n.37C>T) identified in a family with autosomal dominant retinal dystrophy and coloboma. A) Electropherograms showing the 22-nt mature sequence of mir-204. Patient sequence (top) contains the heterozygous mutation (n.37C>T), which segregated amongst affected individuals and the wild-type sequence (bottom) observed in unaffected individuals. The boxed sequence indicates the 7bp seed region. B) Multiple species alignment showing segment of the mir-204 sequence, including the 5p arm, obtained using CLUSTALW software. The human mutation at nucleotide position +37 is indicated in red, underlined sequence denotes the seed region. Hsa-Homo sapiens, ptr-Pan troglodytes, ggo-Gorilla gorilla, mml-Macaca mulatta, bta-Bos Taurus, rno-Rattus norvegicus, mmu-Mus musculus, gga-Gallus gallus, fru-Fugu rubripes, mdo-Monodelphis domestica, pma-Petromyzon marinus C) Predicted secondary structures of wild-type and mutant (n.37C>T) miR-204 precursors obtained using the m-fold algorithm. The nucleotide mutated in the family is indicated in blue and underlined.

Fig. 3. The n.37C>T sequence variation confers altered targeting capabilities to miR-204, as assessed by transcriptome analysis. (A-D) Volcano plots depicting the results of RNA-Seq experiments carried out in ARPE-19 cells transfected with either wt-miR-204 (A-B) or mutated (mut)-miR-204 mimics (C-D). X-axis, expression fold changes (on a log2 scale) vs. control ARPE-19 cells (i.e., negative mimic transfected). Y-axis, statistical significance of expression changes represented as False Discovery Rate (FDR) values on a log10 scale. The black horizontal line indicates FDR=0.05 and the black vertical lines the 10% expression fold change thresholds chosen to identify genes showing significant expression changes. Red dots indicate the genes that show statistically significant down-regulation in each experiment. Green dots indicate the genes that show statistically significant up-regulation in each experiment. Grey dots represent genes that do not display significant expression changes. Black dots in (A) and (C) represent genes that are predicted to be targets of the wt-miR-204 whereas in (B) and (D) represent genes that are predicted to be targets of the mut-miR-204, i.e., carrying the n.37C>T variation. There is a statistically significant enrichment vs. control of, respectively, wt-miR-204 targets in the genes down-regulated in cells transfected with a wt-miR-204 mimic (A) and of mut-miR-204 targets in the genes down-regulated in cells transfected with a mut-miR-204 mimic (D), as determined by hypergeometric analysis.

Fig. 4. Loss of function of miR-204 has a deleterious effect on photoreceptor maintenance and function *in vivo*. Representative frontal eye sections of St38 control (A,C) and Mo-miR-204–injected (B,D) medaka fish embryos immunostained with anti-Rhodopsin and Zpr-1 antibodies (green). Sections are counterstained with DAPI (blue). We observed a significant reduction in the intensity of rhodopsin and Zpr-1 staining in Mo-miR-204–injected medaka fish, compared to controls. A'-D' are higher magnifications of the areas marked by the white dashed boxes in A-D. E) Intensity response curves of mean b-wave amplitude (± SEM) of control and Mo-miR-204 injected larvae (n=30). The b-wave amplitudes of morphant larvae are significantly smaller respect to controls over the 5 units of intensity tested. (F-H) Cell proliferation is not altered in miR-204 morphant embryos. (F, G) Frontal vibratome sections of St30 control and Mo-miR-204 injected embryos immunostained with antiphospho-histone H3 (P-H3) antibodies. (H) Quantification of PH3-positive cells in the retina of the control or Mo-miR-204 injected embryos at different

embryonic stages as indicated. No significant changes were detected between morphants and controls. Red arrows, P-H3-positive cells. (I-K) Frontal vibratome sections of TUNEL-stained control and miR-204 morphant embryos. I-J) A significant increase of photoreceptor cell death in miR-204 morphant eyes was observed when compared to control as also illustrated in the inset that represents a higher magnification of the area marked by the dashed box in D. (K) Quantification of TUNEL-positive cells in the retina of control or Mo-miR-204-injected embryos at different embryonic stages; blue arrows, TUNEL-positive cells; *** =$P<0.0001$ in $\chi 2$ tests. Other abbreviations: OS, Outer Segment of photoreceptors; ONL, Outer Nuclear Layer; INL, Inner Nuclear Layer. Scale bars: 20 μm.

Fig. 5. The n.37C>T miR-204 mutation has a deleterious effect in vivo. (A-C) Bright-field microscopy images of lateral views eyes from control- (A), mut-miR-204- (B) and wt-miR-204- (C) injected embryos. Representative frontal eye sections, immunostained with an anti-Rhodopsin (D-F; green) and ZPR-1 (G-I; green) antibodies, from st38 control (D,G), mut-miR-204-injected (E,H) and wt-miR-204-injected (F,I) medaka fish. Sections are counterstained with DAPI (blue). We observed a significant reduction in the staining of both photoreceptor rods and cones in mut-miR-204–injected medaka fish as compared with control and wt-miR-204-injected animals.

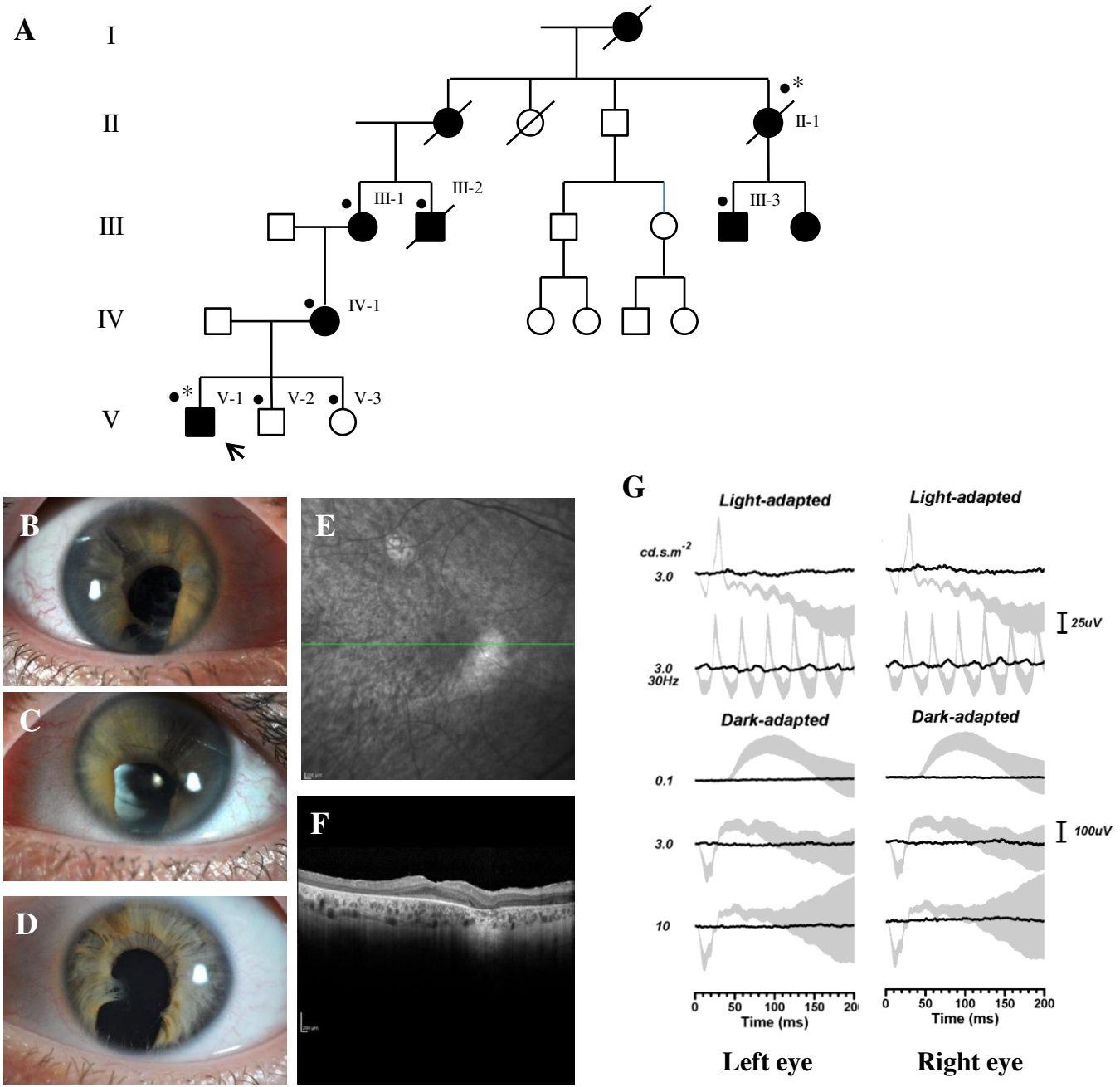
A
I
II
III
IV
V
II-1
III-1
III-2
III-3
IV-1
V-1
V-2
V-3
B
C
D
E
F
G
Light-adapted
Light-adapted
cd.s.m-2
3.0
25uV
3.0
30Hz
Dark-adapted
Dark-adapted
0.1
3.0
10
100uV
0
50
100
150
200
Time (ms)
Left eye
Right eye

Figure 1

A

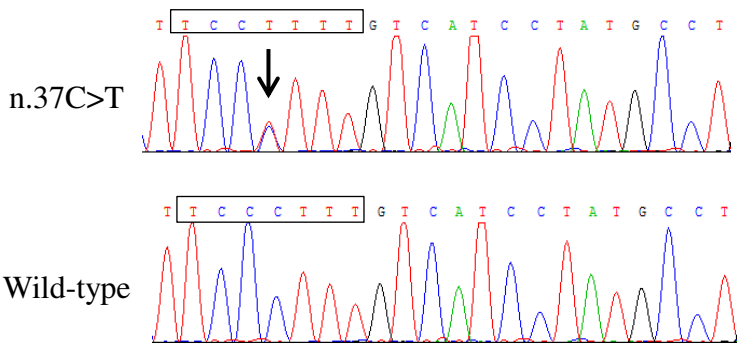

B

```
hsa-mir-204     GUGACUCGUGGACUUCCCUUUGUCAUCCUAUGCCUGAGAAU
ptr-mir-204     GUGACUCGUGGACUUCCCUUUGUCAUCCUAUGCCUGAGAAU
ggo-mir-204     GUGACUCGUGGACUUCCCUUUGUCAUCCUAUGCCUGAGAAU
mml-mir-204     GUGACUCGUGGACUUCCCUUUGUCAUCCUAUGCCUGAGAAU
bta-mir-204     GUGACUCGUGGACUUCCCUUUGUCAUCCUAUGCCUGAGAAU
rno-mir-204     GUGACUCGUGGACUUCCCUUUGUCAUCCUAUGCCUGAGAAU
mmu-mir-204     --------UGGACUUCCCUUUGUCAUCCUAUGCCUGAGAAU
gga-mir-204     GUGACCCGUGGACUUCCCUUUGUCAUCCUAUGCCUGAGAAU
fru-mir-204     GUGACCUGUGGGCUUCCCUUUGUCAUCCUAUGCCUGGAGCU
mdo-mir-204     GUGACCUGUGGGCUUCCCUUUGUCAUCCUAUGCCUGGAAAU
pma-mir-204     -----UGGAGGGAUUCCCUUUGUCAUCCUAUGCCUGUAAUC
                      **   **********************
```

C

hsa-miRNA204 wt — Initial ΔG = -42.30

```
                      20          30          40          50          60
5'GGCUACAGUCUUUCU   -  -    UCG     U          A     U    GAGAAUA
                UCA UG UGAC   UGGAC UCCCUUUGUC UCCUA GCCU       \
                GGU AC ACUG   ACUUG AGGGAAACGG AGGGU CGGA       U
3'----------C----   C  U    UUA     C          A     -    GGAAGUA
          110           100         90         80         70
```

hsa-miRNA204 (n.37C>T) — Initial ΔG = -39.60

```
                      20          30          40          50          60
5'GGCUACAGUCUUUCU   -  -    UCG     U          A     U    GAGAAUA
                UCA UG UGAC   UGGAC UCCUUUUGUC UCCUA GCCU       \
                GGU AC ACUG   ACUUG AGGGAAACGG AGGGU CGGA       U
3'----------C----   C  U    UUA     C          A     -    GGAAGUA
          110           100         90         80         70
```

Figure 2

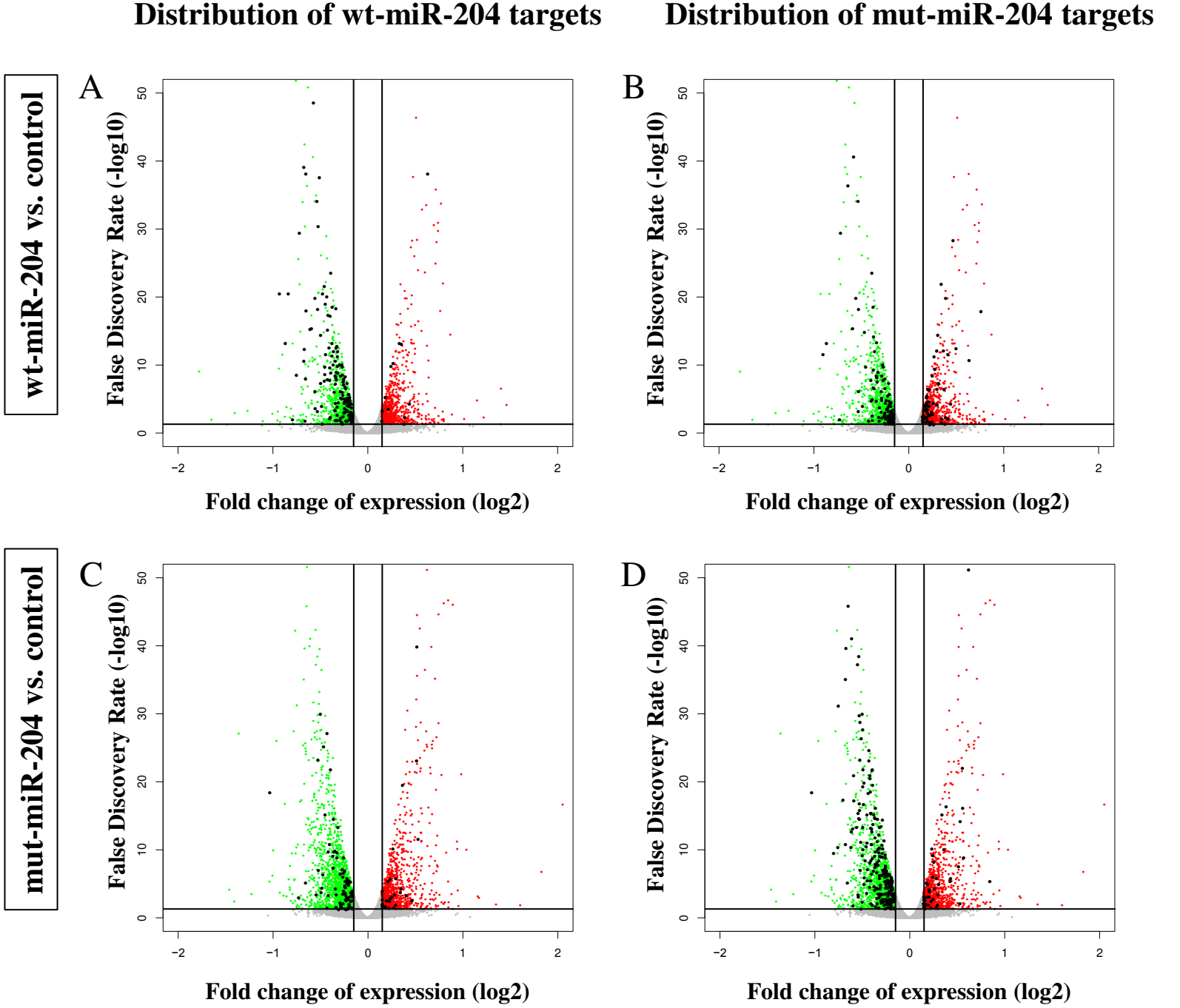
Distribution of wt-miR-204 targets
Distribution of mut-miR-204 targets
wt-miR-204 vs. control
mut-miR-204 vs. control
A
B
C
D
False Discovery Rate (-log10)
Fold change of expression (log2)
0
10
20
30
40
50
−2
−1
0
1
2

Figure 3

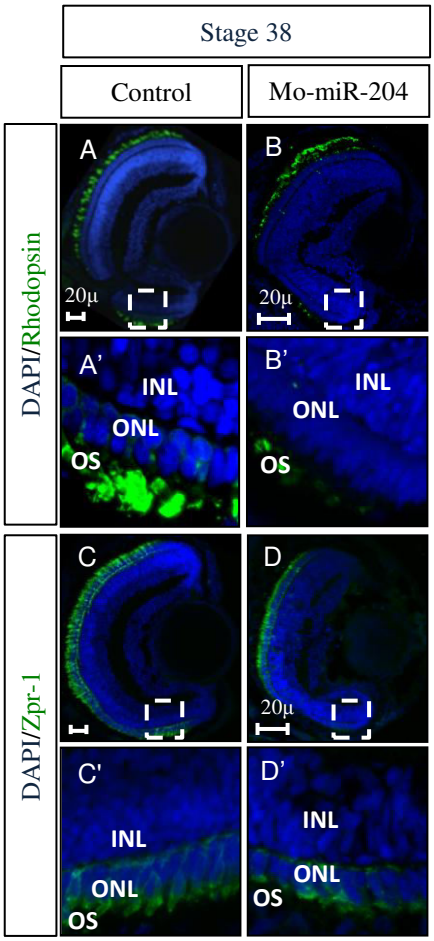

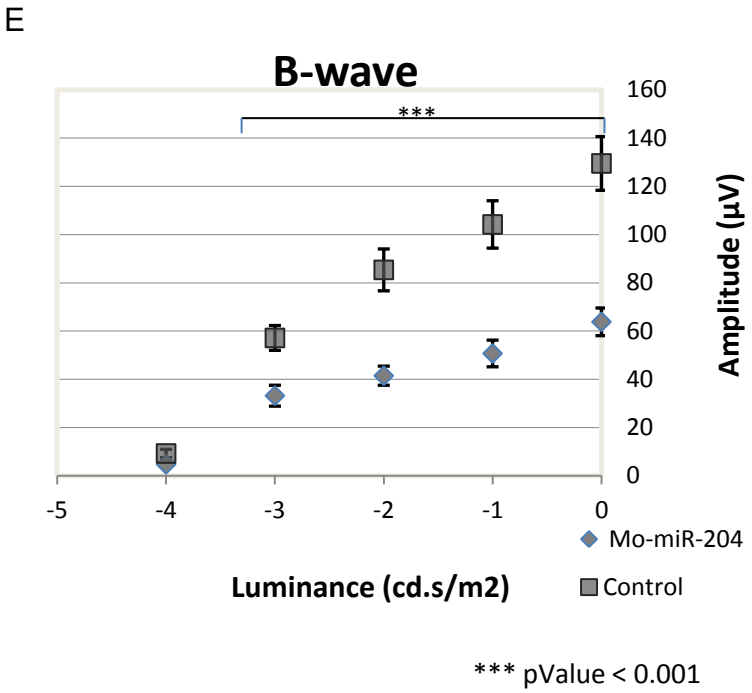

*** pValue < 0.001

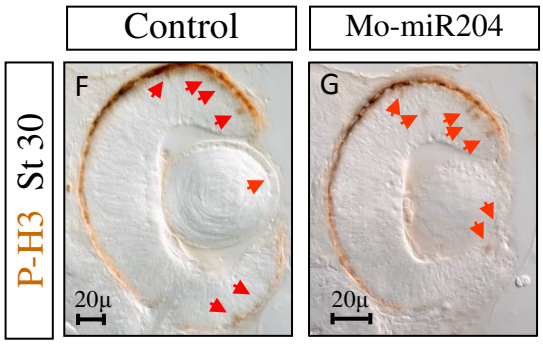

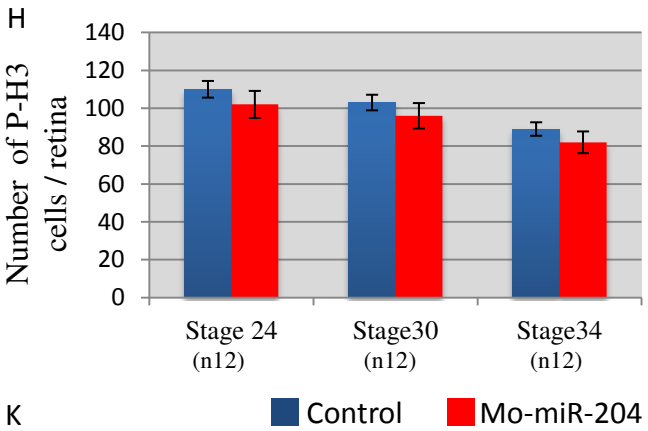

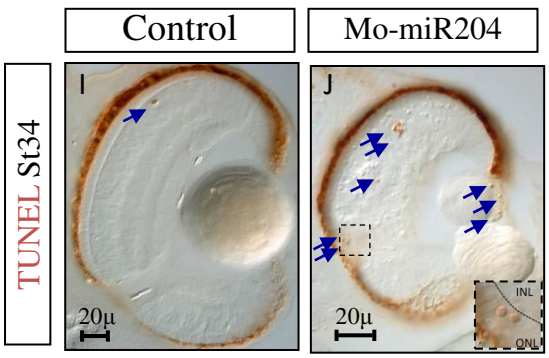

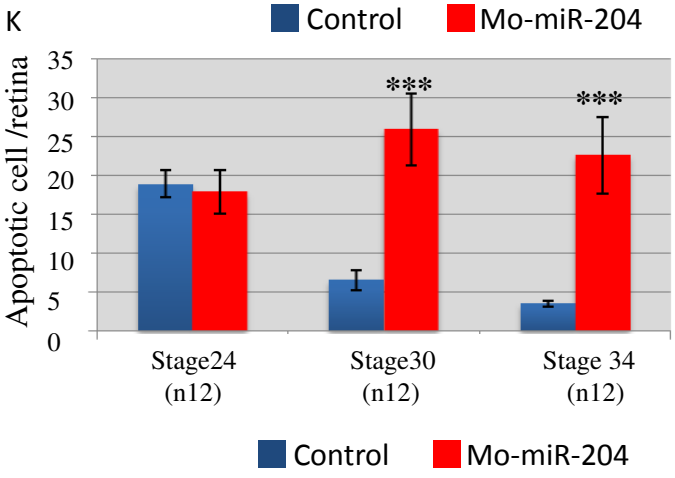

Figure 4

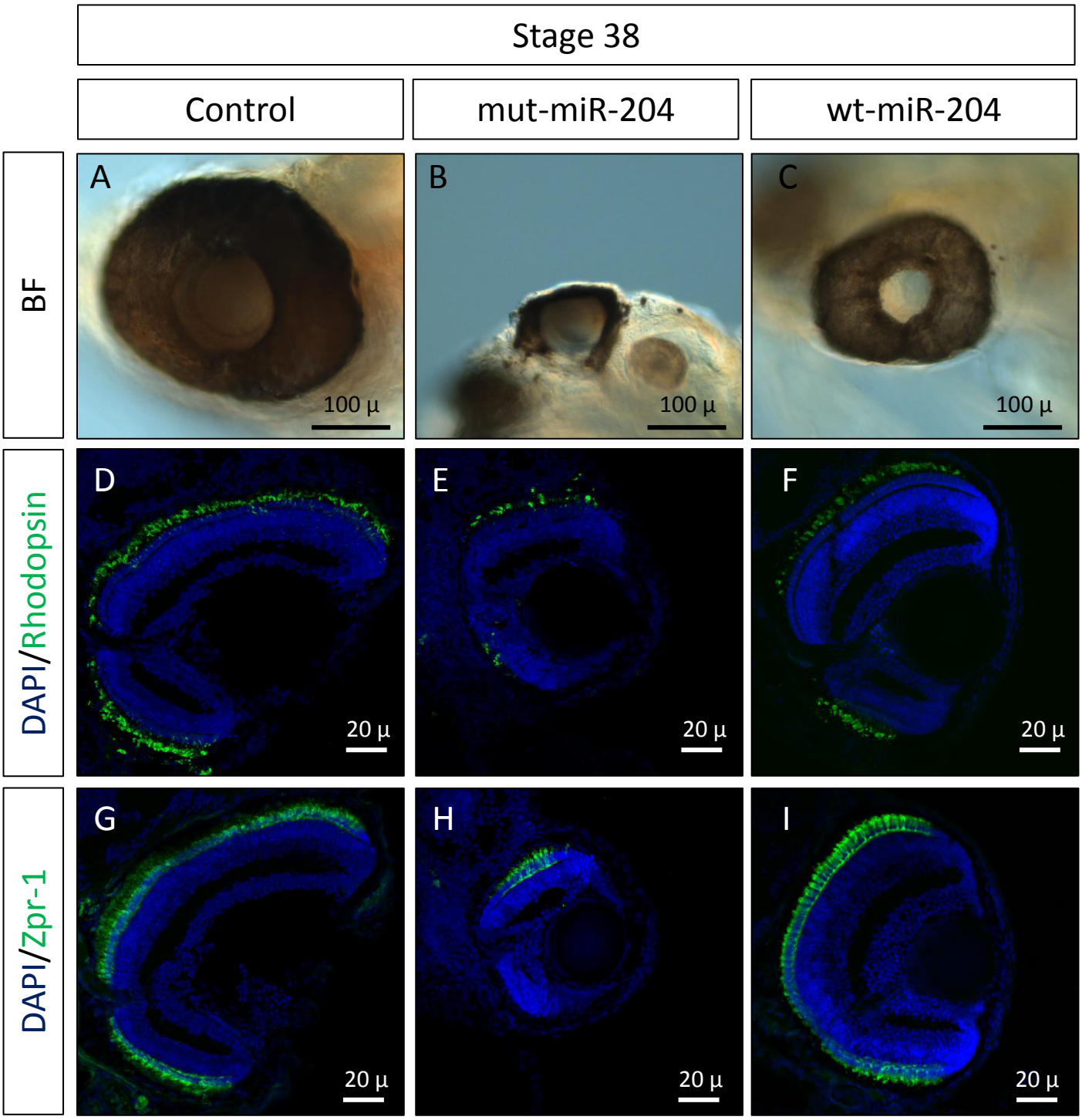
Stage 38
Control
mut-miR-204
wt-miR-204
BF
DAPI/Rhodopsin
DAPI/Zpr-1
A
B
C
D
E
F
G
H
I
100 µ
20 µ

Figure 5